

Bring Gait Lab to Everyday Life: Gait Analysis in Terms of Activities of Daily Living

Diliang Chen¹, Yi Cai¹, Xiaoye Qian¹, Rahila Ansari, Wenya Xu²,
Kuo-Chung Chu, and Ming-Chun Huang³

Abstract—With the development of the Internet of Things (IoT), wearable technologies have been proposed to measure gait parameters in everyday life. However, since both diseases and activities could influence gait patterns, clinicians cannot use the measured gait parameters for clinical applications without knowing the corresponding activities. To address this problem, a novel gait analysis method—“gait analysis in terms of activities of daily living (ADLs)” —was proposed based on a wearable Smart Insole system. Twenty six gait parameters were extracted to realize a systematic gait analysis. Novel activity recognition algorithms based on characteristics of human gait were proposed to recognize ADLs, including “sitting,” “standing,” “walking,” “running,” “ascend stairs,” and “descend stairs” with high accuracy and low computation load. To evaluate the performance of “gait analysis in terms of ADLs,” an experiment consisting of a sequence of different ADLs was designed to simulate the scenario of everyday life. In the result, gait parameters measured during different activities were automatically highlighted with different colors, which made it easy to see whether the gait pattern change was caused by activities or diseases. Besides, a refined gait analysis could be realized by individually extracting and analyzing the gait parameters of a specific activity. The results indicate that “gait analysis in terms of ADLs” is a feasible method to reach the aim of bringing gait lab to everyday life.

Index Terms—Activity recognition, gait analysis, ground reaction force (GRF), smart insole, wearable healthcare.

I. INTRODUCTION

GAIT analysis is a systematic study of human motion [1]. For individuals with diseases that affect the locomotor ability, gait analysis is helpful to make detailed diagnoses,

Manuscript received August 17, 2019; revised October 24, 2019; accepted November 9, 2019. Date of publication November 19, 2019; date of current version February 11, 2020. This work was supported in part by the National Science Foundation under Grant NSF-1664368, in part by the Ohio Bureau of Workers’ Compensation: Ohio Occupational Safety and Health Research Program, and in part by the IoT Collaborative and the Cleveland Foundation. (Corresponding author: Ming-Chun Huang.)

D. Chen, Y. Cai, X. Qian, and M.-C. Huang are with the Department of Electrical Engineering and Computer Science, Case Western Reserve University, Cleveland, OH 44106 USA (e-mail: dxc494@case.edu; yxc757@case.edu; xxq82@case.edu; mxh602@case.edu).

R. Ansari is with the Department of Neurology, Case Western Reserve University, Cleveland, OH 44106 USA, and also with the Department of Neurology, Louis Stokes Cleveland VA Medical Center, Cleveland, OH 44106 USA (e-mail: rxa26@case.edu).

W. Xu is with the Department of Computer Science and Engineering, University at Buffalo, State University of New York, Buffalo, NY 14260 USA (e-mail: wenyaoxu@buffalo.edu).

K.-C. Chu is with the Department of Information Management, National Taipei University of Nursing and Health Sciences, Taipei 11219, Taiwan (e-mail: kcchu@ntunhs.edu.tw).

Digital Object Identifier 10.1109/JIOT.2019.2954387

plan optimal treatment, and evaluate rehabilitation outcomes. For example, for neural system diseases, such as Parkinson’s disease (PD), degrees of gait variability (a parameter for gait analysis) is increased with the disease severity [2]. This makes gait variability a sensitive parameter to evaluate and optimize treatment performance.

A variety of methods could be used to evaluate gait performance in clinical practice. The visual observation method is typically used to determine gait disorders and to evaluate treatment outcome [3]–[5]. However, the accuracy of the subjective result given by visual observation relies on the experience of the clinician who performs the gait assessment, which leads to poor reliability [6], [7]. Quantitative and standardized clinical test, such as timed up and go (TUG) was a complement to the visual observation method [3]. However, performance of the TUG test is limited by the following limitations.

- 1) TUG tests are performed in clinical settings, which cannot accurately reflect the gait performance of a subject in daily life. In gait laboratory or clinical settings, people are aware of the “test” situation, and thus are more conscientious of their performance, which usually results in better performance [8]. In addition, the lab environment does not replicate living conditions, which would also influence the testing results [8].
- 2) Gait performances in different functional tasks, such as “walking” and “turning” are important for disease diagnoses and research, but they cannot be analyzed separately in TUG [8], [9].
- 3) TUG tests only focus on the time variable which is insufficient to detect relevant subtle but important gait abnormalities such as changes in gait variability [10].

To overcome the above limitations, a novel wearable gait analysis method—“gait analysis in terms of activities of daily living (ADLs)” —was proposed based on a Smart Insole system to realize gait analysis in everyday life. Through integrating a pressure sensor array for plantar pressure sensing and an inertial measurement unit (IMU, including accelerometer and gyroscope) for foot motion measurement, Smart Insole could systematically quantify gait performance with 26 gait parameters, including temporal gait parameters, force related gait parameters, turning related gait parameters, gait variability, and gait symmetry. Since both diseases and activities could influence gait patterns, clinicians cannot use the measured gait parameters for clinical applications without knowing the corresponding activities. Therefore, ADLs recognition was realized

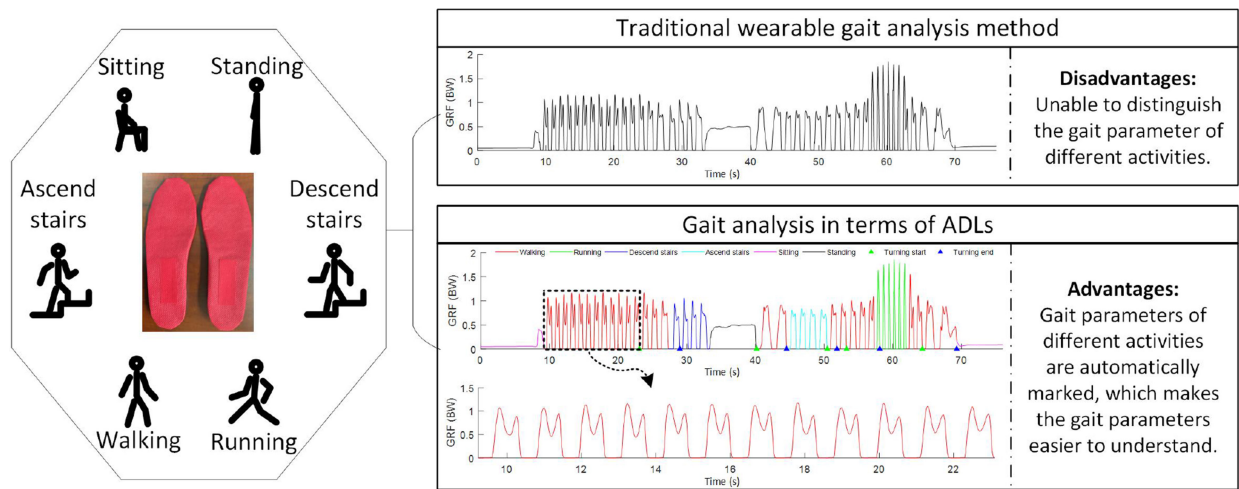


Fig. 1. Advantage of “gait analysis in terms of ADLs.” Icon persons indicate the activities that could be recognized by Smart Insole. GRF recorded during a sequence of different ADLs was used as an example to compare the effect of the traditional wearable gait analysis method and “gait analysis in terms of ADLs.” The red curve in the black dashed rectangle was the GRF recorded during straight walking, which was taken as an example to show that gait parameters of different ADLs could be extracted and analyzed separately.

with Smart Insole to enable “gait analysis in terms of ADLs.” As shown in Fig. 1, six icon persons were used to show the ADLs that could be recognized by Smart Insole. Ground reaction force (GRF) measured during a sequence of different ADLs was taken as an example to show the advantage of “gait analysis in terms of ADLs” over traditional wearable gait analysis methods. The unit of GRF is body weight (BW). For traditional wearable gait analysis methods, although GRF could be measured during different ADLs, GRF of different ADLs cannot be distinguished and the measured GRF cannot be used for clinical applications. For “gait analysis in terms of ADLs,” GRF of different activities were automatically marked with different colors, which makes it easy to see whether the change of GRF patterns is caused by activities or diseases. In addition, gait parameters of a specified activity could be automatically extracted for analyzing individually to enable a refined gait analysis. For example, the GRF in the black dashed rectangle was measured during straight walking, which could be automatically extracted for analyzing individually. Therefore, “gait analysis in terms of ADLs” is a feasible method to realize the aim of bringing gait lab to everyday life. The contributions of this article are as follows.

- 1) Proposed a novel gait analysis method—“gait analysis in terms of ADLs” to fill the gap that limits the application of gait analysis in everyday life. Gait parameters of different ADLs could be distinguished automatically, and could be extracted for analyzing individually.
- 2) Proposed a “stride” based data segmentation method to prepare data for the activity recognition algorithm. This method converts the activity recognition problem of a time period to the activity recognition problem of each “stride” in the time period. In addition, this data segmentation method could recognize the boundary that separates two different activities.
- 3) Proposed an efficient activity recognition algorithm based on characteristics of human gait, which could achieve high accuracy with low computation load.

- 4) Realized “gait analysis in terms of ADLs” in practice by embedding algorithms for gait parameters calculation and ADLs recognition into a smartphone Application (App).

II. RELATED WORK

With the development of technologies, new gait analysis methods have been proposed to help improve the traditional methods, such as observation method and TUG test. According to Muro-De-La-Herran *et al.* [11], the new gait analysis methods can be classified into two categories: 1) nonwearable methods and 2) wearable methods.

For nonwearable methods, optic sensors and force platforms were usually used for acquiring data for objective gait analysis. Prakash *et al.* [12] used a digital video camera and five passive markers attached to the body joints to build a 2-D joint movement tracking system. Gait analysis is done with a gait analysis model developed using a simulation framework. Wang *et al.* [13] used the second generation Microsoft Kinect to build a 3-D skeleton-based gait database for gait analysis. Commercially available nonwearable gait analysis systems, such as the Vicon camera system and GAITRite force platform were recognized as a gold standard for gait analysis [14], [15]. However, nonwearable methods need a controlled environment where necessary devices, such as cameras and force platforms have to be set up before measurement. Therefore, nonwearable methods are not suitable for gait analysis in a free-living environment.

For wearable methods, wearable sensors, such as accelerometer, gyroscope, magnetometers, and pressure sensors were frequently used for acquiring various signals for gait parameters calculation. Since wearable sensors can be worn on the body directly and work in a free-living environment, wearable gait analysis methods have the potential to be applied in everyday life. IMU sensors were usually placed on thigh, shank, and foot to record data for gait analysis [16], [17]. However, only

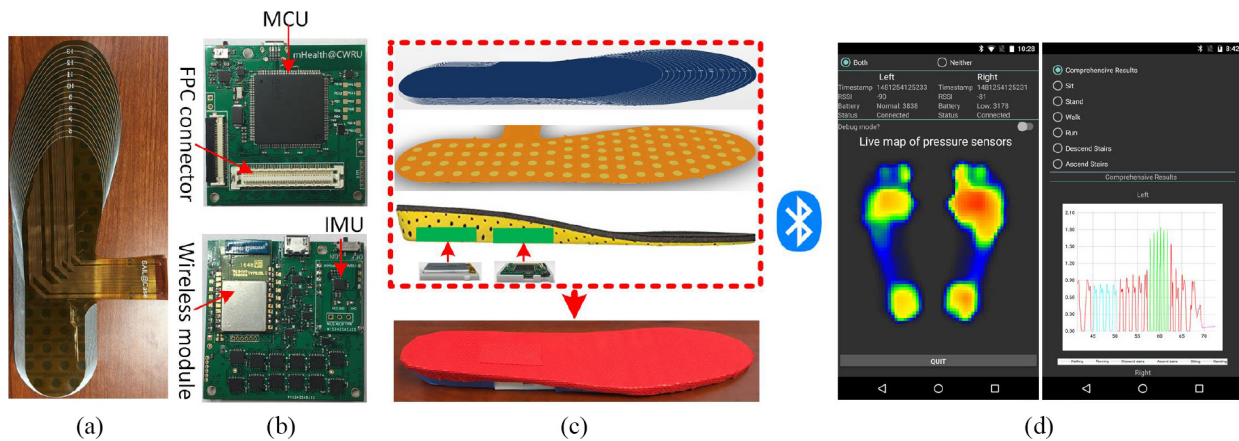


Fig. 2. Hardware and software of the Smart Insole system. (a) Insole shaped customizable pressure sensor array. (b) Circuit board for signal acquisition and data transmission. (c) Assembly structure of Smart Insole. (d) Smartphone App for gait parameters calculation, ADLs recognition, and results display.

IMU sensors cannot supply force related gait parameters. Since most human motion is performed with the support of both feet, many researches focus on the gait analysis through foot motion measurement. F-Scan [18] is a well known commercially available insole shaped system for gait analysis. However, F-Scan needs users to bind signal processing devices to lower limbs. Since people prefer sensors embedded into their clothing or accessories than wearing a technology separately [19], binding an extra device to human body would decrease the willingness of people to use this technology during everyday life. Saito *et al.* [20] proposed a more integrated insole shaped device for measuring plantar pressure during daily human activities, which does not need to attach extra devices to human body. However, the design of Saito *et al.* only includes pressure sensors which cannot measure turning related gait parameters. Wang *et al.* [21] further improved the design of Saito *et al.* by adding an IMU sensor which makes it possible to measure comprehensive gait parameters. However, one shortcoming of these two designs is that there are only several pressure sensors on the insole, which makes it difficult to measure important force related gait parameters such as the center of pressure. Another shortcoming is that the pressure sensors are nonuniformly deployed on fixed locations, which makes the design noncustomizable. However, noncustomizable designs would significantly increase the manufacturing cost, because different designs have to be built to meet personalized requirements on different shapes and sizes. To decrease the manufacturing cost, the solution of many commercial products is to make a tradeoff by supplying limited sizes to consumers. For example, both ARION smart insole [22] and Stridalyzer insole [23] only supply four different sizes. However, it is obvious that limited sizes cannot ensure a good fit for people with different foot shapes and sizes, then influence the measurement accuracy.

In addition to the shortcomings of wearable system design, one research gap is that most existing wearable solutions for gait analysis only focus on measuring gait parameters in free-living environments, which is not enough to supply understandable gait parameters for clinicians. Since both diseases and activities could change the pattern of gait parameters,

without knowing the corresponding activities, the measured gait parameters cannot be used in clinical applications.

To address the shortcomings related to system design, an unobtrusive and customizable Smart Insole system was proposed for a comprehensive gait analysis. To fill the gap that limits the application of gait analysis in free-living environments, the new technologies of gait analysis and activity recognition were explored to realize “gait analysis in terms of ADLs.”

III. METHOD

In this section, details of the Smart Insole system, algorithms for gait parameters calculation, and activity recognition were specified.

A. Smart Insole System Design

In this article, Smart Insole is an important system for realizing “gait analysis in terms of ADLs.” Fig. 2 shows the hardware system [Fig. 2(a)–(c)] for signal acquisition and data wireless transmission, and the software system [Fig. 2(d)] for gait parameters calculation, ADLs recognition, and results display. Fig. 2(a) shows an insole shaped pressure sensor array for measuring the plantar pressure signal. A commercially available piezo-resistive fabric material made by EeonTex was used for designing the pressure sensor array [24]. Just like normal fabric materials, it is thin (with a thickness of 0.8 mm), light-weight (with a weight of 170 g/m²), and flexible. One limitation of this material is that its pressure sensitivity is not perfectly uniform. As shown in a former research [25] about the pressure sensor array, the mean and maximum variance of the pressure sensitivity was 4.6% and 7.9%, respectively. Although this piezo-resistive fabric is not perfect, it might be good enough for applications focusing on the pattern of GRF [25]. To decrease the manufacturing cost, a customizable design was applied to the pressure sensor array, which makes it possible for the sensor array to be trimmed to fit feet with sizes from 5.5 U.S. to 14 U.S. [25], [26]. Up to 96 pressure sensors were uniformly distributed on the pressure

sensor array, which ensures a high spatial resolution for plantar pressure measurement. For details of the design method and mechanism of the pressure sensor array, please refer to the former research [25]. Fig. 2(b) shows a circuit board for signal acquisition and data wireless transmission. A flexible printed circuit (FPC) connector is used to connect the pressure sensor array for pressure signal acquisition. The IMU sensor, including accelerometer and gyroscope, is used to measure the foot motion. A microcontroller unit (MCU) is used to control the process of signal acquisition and data transmission. The sample rate for sensor data acquisition is 30 Hz. Wireless module (classic Bluetooth) is used to transfer the acquired sensor data to a smartphone App for further processing. Considering the fact that people prefer sensors embedded into their clothing or accessories than wearing a technology separately [19], all the hardware systems were packed into an insole shaped package which makes the use of Smart Insole similar to normal insoles. This unobtrusive design would contribute to the measure of nature gait during everyday life. The assembly structure shown in Fig. 2(c) describes the method to assemble a Smart Insole that looks the same as a normal insole from outside. Smart Insole is with a four-layer design. The insole shaped package shown on the third layer is the main structure of Smart Insole. The Li-ion battery (3.7 V, 1000 mAh) and circuit board shown on the fourth layer are protected with 3-D printed cases and embedded into the green area of the insole package. The pressure sensor array shown on the second layer is attached to the top surface of the insole package. Finally, a fabric material shown on the first layer is used to cover the pressure sensor array to ensure the wear comfort. The smartphone App shown in Fig. 2(d) is used to further process (gait parameters calculation, ADLs recognition) the sensor data acquired from the Smart Insole hardware, and display the processed results. Two screenshots were used to show parts of the App functions. The screenshot on the left shows a real-time plantar pressure map. The screenshot on the right demonstrates the effect of “gait analysis in terms of ADLs.” The plot shown was the GRF measured during a sequence of different activities. Since different activities could be recognized automatically by the smartphone App, the GRF measured during different activities were marked automatically with different colors to make it easy for clinical professionals to understand the results.

B. Gait Parameters Calculation

As shown in Table I, Smart Insole could quantify gait performance with 26 gait parameters. In this section, the method for estimating BW and algorithms for calculating gait parameters, including temporal gait parameters, force related gait parameters, gait variability, gait symmetry, and turning related gait parameters were specified.

1) *Body Weight Estimation*: Different people have different BW which could directly influence the measured GRF and other force related gait parameters. However, changes in gait parameters caused by BW do not correlate with an abnormal gait. In addition, the pressure sensitivity of the piezo-resistive material used for plantar pressure sensing is not perfectly uniform, which could lead to differences in the GRF measurement

with different Smart Insoles. Therefore, to avoid the influences of BW on gait parameters presentation and avoid the influences of the nonuniform pressure sensitivity on the GRF measurement, BW was used to normalize GRF.

Before using Smart Insole for gait analysis, the BW should be estimated with the left and right Smart Insoles separately. In the process of measuring BW, the people should wear a pair of Smart Insole without carrying additional load and stand steadily with one foot for a while (e.g., 5 s), then stand steadily with the other foot for the same time. Finally, the mean GRF of the left and the mean value of the right Smart Insole in the measuring time were the BW for normalizing the GRF measured with the left and right Smart Insole, respectively.

2) *Temporal Gait Parameters*: The gait cycle of a foot includes a stance phase when the foot is in contact with the ground, and a swing phase when the foot is in the air. During the swing phase, since there is no extra pressure applied on the pressure sensor array except for some minor contact pressure, the measured GRF would be small. When it comes to the stance phase, the force to support the BW and secure the safe movement would be applied to the pressure sensor array, and then the measured pressure would be significantly increased. Based on these characteristics, some published researches used a fixed threshold to discriminate the stance and the swing phase [27]. However, a fixed threshold does not work well on the GRF samples measured at the very start or end stage of a stance phase, when the amplitude could be below the fixed threshold. In this article, an adaptive threshold was proposed based on the amplitude of swing samples to discriminate the stance and the swing phase. Fig. 3(a) shows the GRF during a normal walking activity. As expected, samples of GRF during the swing phase are near zero, and increased significantly during the stance phase. To find the adaptive threshold, a fixed threshold (e.g., 0.0300 BW) was used to roughly discriminate the stance and swing samples. Black dots indicate the GRF samples over the fixed threshold. Red dots indicate the first and last GRF sample of a stride that are below the fixed threshold, and blue dots indicate the remaining GRF samples that are below the fixed threshold. Since the samples indicated with red dots could be the start or end of a stance phase, they were excluded from the data set for adaptive threshold calculation. Therefore, only the samples indicated with blue dots were used to estimate the adaptive threshold based on (1). n_{swing} indicates the number of swing samples used for the adaptive threshold estimation, and σ_{swing} indicates the standard deviation of the GRF during the swing phase. The distribution of GRF in the swing phase is assumed to fit normal distribution. According to the empirical rule of normal distribution, nearly all the data (99.73%) would lie within three standard deviations of the mean. Therefore, the GRF samples higher than the adaptive threshold are more likely to be samples of a stance phase

$$\text{Adaptive Threshold} = \frac{1}{n_{\text{swing}}} \sum_{k=1}^{n_{\text{swing}}} \text{GRF}_k + 3 * \sigma_{\text{swing}}. \quad (1)$$

As shown in Fig. 3(b), there are five samples located between the fixed and adaptive (i.e., 0.0099 BW) threshold.

TABLE I
GAIT PARAMETERS PROVIDED BY SMART INSOLE

No.	Gait parameters	Description	Medical value	
1	Gait cycle time (in s)	Time interval between two successive occurrences of one of the repetitive events (e.g. initial contact) of the same foot. This parameter is calculated for both feet.		
2	Step time (in s)	Time duration from the initial contact of one foot to the initial contact of the other foot. This parameter is calculated for both feet.		
3	Swing time (in s)	Time duration between the last contact of one stride and the initial contact of the subsequent stride of the same foot. This parameter is calculated for both feet.		
4	Stance time (in s)	Time duration between the initial and last contact of a stride. This parameter is calculated for both feet.		
5	Single support time (in s)	Time duration in a gait cycle when only one foot is in contact with the ground. This parameter is calculated for both feet.		
6	Double support time (in s)	Time duration in a gait cycle when both feet are in contact with the ground. This parameter is calculated for both feet.		
7	Cadence(in steps/min)	The number of steps in a minute.		
8	Center of Pressure (CoP, in cm)	The average of pressure weighted sensor location in both X- and Y-axis. These parameters are calculated for both feet.	Basic gait parameters used to describe the human gait quantitatively.	
9	GRF (in BW)	Summation of the force measured by all the pressure sensors under foot. This parameter is calculated for both feet.		
10	GRF of the forefoot (in BW)	Summation of the force measured by all the pressure sensors in the forefoot area. This parameter is calculated for both feet.		
11	GRF of the midfoot (in BW)	Summation of the force measured by all the pressure sensors in the midfoot area. This parameter is calculated for both feet.		
12	GRF of the hindfoot (in BW)	Summation of the force measured by all the pressure sensors in the hindfoot area. This parameter is calculated for both feet.		
13	Location of the maximum GRF of the forefoot (in cm)	Location of the maximum GRF in the forefoot area, which is described with coordinates in both X- and Y-axis. This parameter is calculated for both feet.		
14	Location of the maximum GRF of the midfoot (in cm)	Location of the maximum GRF in the midfoot area, which is described with coordinates in both X- and Y-axis. This parameter is calculated for both feet.		
15	Location of the maximum GRF of the hindfoot (in cm)	Location of the maximum GRF in the hindfoot area, which is described with coordinates in both X- and Y-axis. This parameter is calculated for both feet.		
16	Weight-acceptance force (in BW)	Amplitude of the first peak in the plot of GRF during the stance phase. This parameter is calculated for both feet.		
17	Push-off force (in BW)	Amplitude of the second peak in the plot of GRF during the stance phase. This parameter is calculated for both feet.		
18	Mid-stance force (in BW)	Amplitude of the valley in the plot of GRF during the stance phase. This parameter is calculated for both feet.		
19	Weight-acceptance rate (in BW/s)	The average changing rate of GRF from the initial contact to the first peak of GRF. This parameter is calculated for both feet.		
20	Push-off rate (in BW/s)	The average changing rate of GRF from the second peak of GRF to the end of the stance phase. This parameter is calculated for both feet.		
21	Gait variability	Stride to stride fluctuations in gait parameters. This parameter could be calculated with all the above basic gait parameters.		Gait variability is a marker of gait stability and cortical gait control.
22	Gait symmetry	A measure of parallels between two lower limbs. This parameter could be calculated with all the above basic gait parameters.		Gait symmetry can provide unique insight about the gait control.
23	Turning time (in s)	Time duration between the start of the first turning step to the end of the last turning step.		Turning gait parameters are sensitive to gait related pathologies such as PD.
24	Turning steps	The number of steps used to complete a turn		
25	Turning angle (in degree)	The angle amplitude changed from the start to the end of a turn		
26	Turning angle of each step (in degree)	The angle amplitude changed in each stride.		

Since the amplitude of these five samples is much higher than the amplitude of the swing samples indicated with blue dots, these five samples should belong to the stance phase.

Therefore, the adaptive threshold has a better performance than the fixed threshold for discriminating the stance and swing samples.

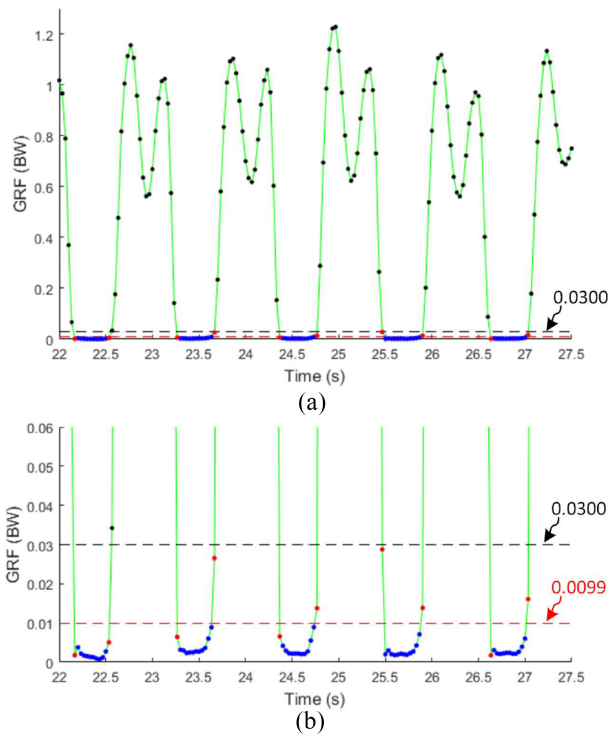


Fig. 3. Dynamic threshold for discriminating stance and swing phases. (a) GRF measured during normal walking. (b) Zoomed in the plot of (a) in range [0 0.0600] to show the effect of the adaptive threshold. The green line indicates the trend of GRF. Each dot indicates a sample of GRF. The black dashed line indicates a regular fixed threshold and the red dashed line indicates an adaptive threshold. Black dots indicate the GRF samples over the fixed threshold. Red dots indicate the first and last GRF samples of a stride that are below the fixed threshold, and blue dots indicate the remaining GRF samples that are below the fixed threshold.

For the other temporal gait parameters, such as “double support time,” “single support time,” “gait cycle time,” and “step time,” the right foot was taken as an example to show the calculating method. As shown in Fig. 4, the double support phase occurs when both feet are in the stance phase, and the single support phase occurs when only one foot is in the stance phase. The gait cycle time is defined as the time interval between two successive occurrences of one of the repetitive events (e.g., initial contact) [1]. Step time could be calculated from the initial contact of one foot to the subsequent initial contact of the other foot.

3) *Ground Reaction Force Related Gait Parameters:*

The characteristics of GRF are important indicators, which can supply additional insights into the pathological gait [28], [29]. Researches showed that the pattern of GRF during walking could reflect the stage of the PD [30]. For the early stages of PD, the amplitude of both GRF peaks (weight-acceptance pressure and push-off pressure shown in Fig. 5) are reduced, and the GRF would have only one single narrow peak in the advanced stages [31]. In addition, researches about the pressure distribution on subareas of the foot showed that, for the diabetic neuropathic foot, there is an increase in the pressure of both the forefoot and hindfoot, and the imbalance of pressure distribution would be increased with the degrees of neuropathy [32]. CoP is commonly used to evaluate balance control,

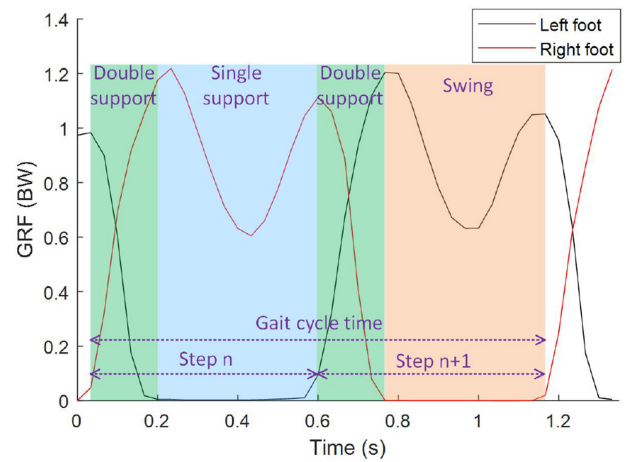


Fig. 4. Method of calculating temporal gait parameters. The black and red line indicates the GRF of the left and right foot during walking, respectively. The areas highlighted with green, blue, and orange colors indicate the double support phase, single support phase, and swing phase, respectively.

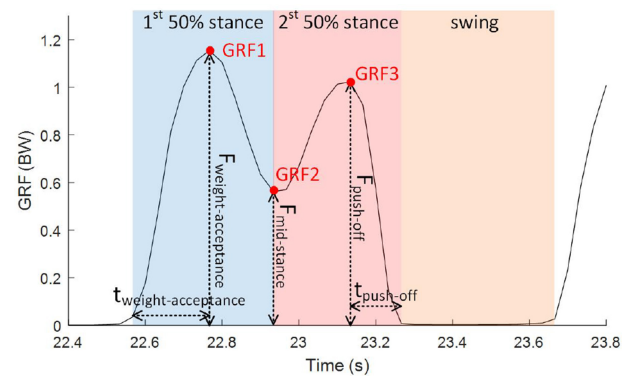


Fig. 5. Locating weight-acceptance force peak, mid-stance force valley, and push-off force peak. From left to right, the red points indicate the location of the weight-acceptance peak (GRF1), mid-stance valley (GRF2), and push-off peak (GRF3), respectively. The blue, red, and orange background indicate the time period corresponding to the first half stance, the second half stance, and the swing phase, respectively.

foot function, and treatment efficacy [33], [34]. In this article, 13 force related gait parameters (shown in Table I) were obtained from each foot.

Two peaks and a valley can be observed in the GRF plot during walking. This is caused by the fact that during walking, the center of mass (COM) of the body has a cyclic acceleration characteristic in the vertical direction, which is directly related to the GRF. In the early stance (weight-acceptance), GRF usually exceeds BW to accelerate COM upward. During mid-stance, the GRF falls below BW to make COM accelerate downward. During the late stance (push-off), GRF is increased again to accelerate the COM upward [35]. Fig. 5 shows the method of finding weight-acceptance peak (GRF1), mid-stance valley (GRF2), and push-off peak (GRF3). For a normal gait cycle, the weight-acceptance and push-off phase takes a similar time length [36]. Therefore, the stance phase was separated into two equal parts first, then the maximum force in the first part is recognized as the weight-acceptance force, and the maximum force in the second part is recognized as the push-off force. Finally, the mid-stance force could be

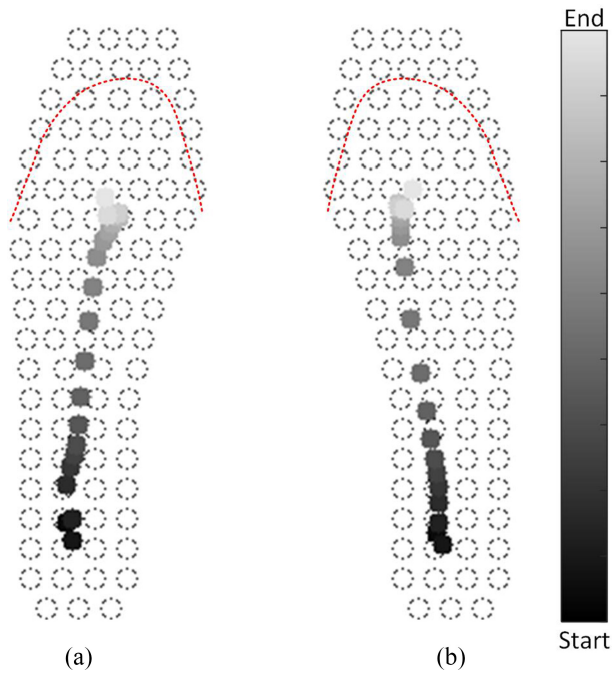


Fig. 6. Location of CoP during the stance phase of the (a) left and (b) right strides. Each grey point indicates one CoP location. Gray level of each point indicates the time when the CoP point occurs. The color bar on the right shows the relation of the grey level and the occurrence time. Black color indicates the beginning of the stance phase, and a whiter color indicates the end of the stance phase. Each black dashed circle indicates the location of a pressure sensor. Red dashed lines indicate the outline of a 10.5 U.S. sized insole used in this article.

located by finding the minimum force between the location of weight-acceptance and push-off force.

The weight-acceptance rate and push-off rate could be calculated with the equation F/t . For the weight-acceptance rate, F is the weight-acceptance force, and t is the time length from the beginning of the stance phase to the occurrence of the weight-acceptance force. Similarly, for the push-off rate, F is the push-off force, and t is the time length from the occurrence of the push-off force to the end of the stance phase.

Horizontal and vertical coordinators of the CoP were calculated with the following equations:

$$\begin{cases} \text{CoPx} = \frac{\sum_{i=1}^n x_i p_i}{\sum_{i=1}^n p_i} \\ \text{CoPy} = \frac{\sum_{i=1}^n y_i p_i}{\sum_{i=1}^n p_i} \end{cases} \quad (2)$$

where CoPx and CoPy refer to the horizontal and vertical coordinate of CoP, respectively; n refers to the number of pressure sensors on each insole; x and y refer to the horizontal and vertical coordinates of a sensor; and p refers to the measured pressure value of a sensor. During the swing phase, since the foot is in the air and has no pressure on the pressure sensor array except the contact pressure, the corresponding CoP is set to the insole center.

A novel vivid presentation method for CoP was shown in Fig. 6. Fig. 6(a) and (b) shows the location of CoP during the stance phase of a left and a right stride, respectively. The gray level of each point indicates the time when the CoP point occurs. Therefore, Fig. 6 could supply not only the information about CoP trajectory, but also information about how the CoP

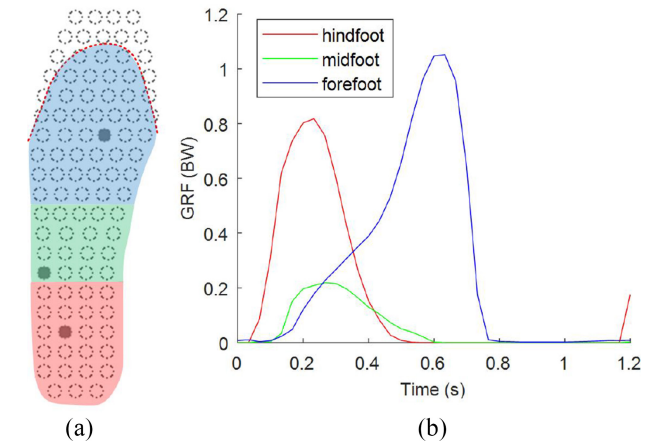


Fig. 7. Pressure measurement for forefoot, midfoot, and hindfoot. (a) Highlights forefoot, midfoot, and hindfoot areas with blue, green, and red colors, respectively. The black dot in each area indicates the location with the highest pressure in that area during a stride. The Red dashed line indicates the outline of the 10.5 U.S. sized insole used in this article. (b) Measured GRF of each area during a gait cycle.

location changes over time. Since the sample rate for the pressure sensor array is fixed, Fig. 6 could also supply an intuitive view of CoP velocity at different locations.

To study the pressure distribution on subareas of the foot, the foot was separated into three areas: 1) forefoot; 2) midfoot; and 3) hindfoot [37]. In foot anatomy, the forefoot consists of phalanges and metatarsal bones; the mid-foot contains navicular, cuboid, and cuneiform bones; and the hindfoot consists of talus and calcaneus bone [38]. As shown in Fig. 7(a), areas of the pressure sensor array corresponding to the forefoot, mid-foot, and hindfoot were highlighted with blue, green, and red background, respectively. Black dots indicate the sensor location with the highest pressure in the corresponding areas. Fig. 7(b) shows the recorded pressure of different areas during a gait cycle.

4) *Gait Variability*: Gait variability is defined as changes in gait parameters from one stride to the next [39]. According to a common assumption, gait variability is inversely related to gait stability [40]. There is growing evidence shows that gait variability is associated with falling [41], [42], frailty [43], and neuro-degenerative diseases such as PD [2]. In addition, researches showed that degrees of gait variability were increased with the severity of diseases, such as PD and Huntington's diseases, which made it a sensitive parameter to evaluate the therapeutic interventions [2].

Coefficient of variation (CoV) is commonly used to describe the variability of gait parameters, which could be calculated with the following equations [44]:

$$\begin{cases} \text{CoV} = \frac{\sigma}{\mu} * 100\% \\ \mu = \frac{1}{N} * \sum_{i=1}^N (V_i) \\ \sigma = \sqrt{\frac{1}{N} \sum_{i=1}^N (V_i - \mu)^2} \end{cases} \quad (3)$$

where, V indicates the gait parameter used for calculating CoV, N indicates the number of samples of a gait parameter used for the calculation, μ and σ indicates the mean and standard deviation of the gait parameter.

5) *Gait Symmetry*: Gait symmetry is a measure of the parallels between the lower limbs, which could provide a unique insight into the walking control function [45]. Gait asymmetry is commonly occurred in people with neurological diseases (e.g., PD and stroke) [46], [47], single leg amputees [48], and knee osteoarthritis [49], etc. There is growing evidence shows that persisting gait asymmetry is associated with many negative consequences, such as challenges to balance control, gait inefficiency, risk of overusing the nonparetic limb, and loss of bone mineral density in the paretic limb [45], [50]. Monitoring gait symmetry could help clinicians learn about the rehabilitation progress of the corresponding diseases and make further treatment decisions [45]. Gait symmetry index (SI) is calculated with the following equation [49]:

$$SI = 2 * \left| \frac{V_{\text{left}} - V_{\text{right}}}{V_{\text{left}} + V_{\text{right}}} \right| * 100\% \quad (4)$$

where, V_{left} and V_{right} indicate the gait parameters of the left and right foot, respectively.

6) *Turning Related Gait Parameters*: Turning is a common but challenging activity in daily life, which needs a complex integration of different control mechanisms [51]. More requirements on the integration of control mechanisms and a higher level of neural control may make turning more sensitive to diseases such as PD than linear walking [51]. This corollary is supported by the fact that PD patients demonstrated a significant slower step and a greater number of steps to finish a turn, but no significant abnormal stride parameters during linear walking [51].

In this article, turning related parameters, such as turning time, turning steps, turning angle, and turning angle of each step were calculated. The start of “turning” is recognized when the turning angle of double feet both exceed an empirical threshold of 15°. Similarly, the end of “turning” is detected when the turning angle of double feet are less than the threshold. The methods for calculating turning related gait parameters were specified in Table I.

C. Activities of Daily Living Recognition

With the methods discussed in Section III-B, gait parameters could be measured in everyday life. In this section, the activity recognition algorithm for recognizing normally occurred ADLs, such as “sitting,” “standing,” “walking,” “running,” “descend stairs,” and “ascend stairs” would be specified.

ADLs recognition algorithms should meet the following requirements to enable “gait analysis in terms of ADLs”: 1) ADLs should be recognized with high accuracy; 2) different activities should be clearly separated during the transition of activities; and 3) ADLs recognition algorithms could run on mobile devices such as smartphones. The first and second requirements could ensure that when analyzing the gait parameter of one activity, the gait parameter of the other activities could be excluded to avoid potentially misleading. The third requirement is necessary for a mobile gait analysis solution in free-living environments. However, many published researches about ADLs recognition with wearable systems showed that it is challenging to recognize activities, such as “walking,” “descend stairs,” and “ascend stairs” with a

high accuracy (e.g., 95%) [52]–[54]. In addition, sliding windows were normally used to segment sequential signals for activity recognition algorithms. Since it is common for a sliding window to cover two different activities during the activities transition period, it is difficult to clearly separate different activities with sliding windows. Besides, many published researches extracted tens of general features, such as mean value, max value, and standard deviation to train a model for ADLs recognition, which made it hard for the model to run on a mobile device [52], [53].

To address the above problems, a novel and effective method was proposed based on the characteristics of human gait. Based on whether strides are necessary for performing an activity, ADLs could be separated into two categories: 1) dynamic activities and 2) quasi-static activities. “Walking,” “running,” “descend stairs,” and “ascend stairs” were recognized as dynamic activities, since these activities need to be performed with strides. On the other hand, since “sitting” and “standing” do not consist of strides, they were recognized as quasi-static activities.

For dynamic activities: 1) to clearly separate different activities during activities transition, a data segmentation method using “stride” as the unit was proposed. For human gait, it is a common sense that one can only perform one activity during a stride. For example, one can perform “walking” or “running” but cannot perform both “walking” and “running” during one stride. Therefore, “stride” based data segmentation method could clearly separate different activities. This data segmentation method could also simplify the ADLs recognition problem in a time period to the problem of recognizing the activity of each stride in the time period and 2) to increase the accuracy of ADLs recognition and reduce the computation load, only three efficient features were extracted from each stride based on human gait characteristics. These three features were “foot contact pitch,” “foot contact pitch—GRF2 pitch,” and “percentage of double support time.” “Foot contact pitch” is the pitch angle at the time when foot initially contacts the ground, “GRF2 pitch” is the pitch angle at midstance, which is near zero for flat surfaces and normal postures, but shifts from zero during uneven surfaces or abnormal postures. “Foot contact pitch—GRF2 pitch” is introduced to increase the classification reliability. “Percentage of double support time” is the percentage of double support time over the total gait cycle time. Different activities have different characteristics. Fig. 8 shows the characteristics of each posture, which could be used to discriminate the dynamic activities. Fig. 8(a)–(c) shows the posture of “walking,” “ascend stairs,” and “descend stairs” at the time when the foot is initially contacting the ground. It is obvious that the position of forefoot is significantly higher than hindfoot for “walking,” while forefoot position is significantly lower than hindfoot for “descend stairs,” and the foot is almost flat for “ascend stairs.” These posture differences could lead to significant differences on the value of “foot contact pitch” [55]. As shown in Fig. 8(d), the character that could be used to discriminate “running” from “walking,” “descend stairs,” and “ascend stairs” is the “percentage of double support time.” For running, the double support phase is replaced by the double float phase when neither foot is touching the

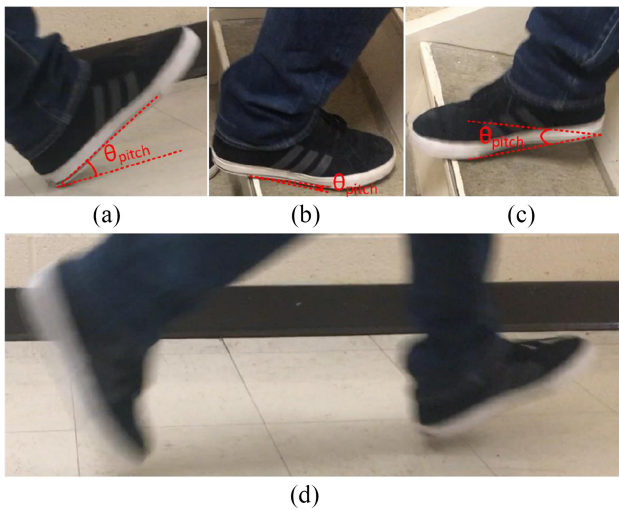


Fig. 8. Characteristics for dynamic activities recognition. Pitch angle of (a) walking, (b) ascend stairs, (c) descend stairs at the initial contact event, and (d) the double float phase during running.

ground [56]. Therefore, the “percentage of double support time” of “running” would be significantly lower than the other three activities. Linear support vector machine (SVM) was used to train an activity recognition model with these three features for ADLs recognition.

On the other hand, for quasi-static activities, “sitting” and “standing” could be recognized based on the measured plantar pressure of both feet. When the measured total pressure is decreased to a value of less than 0.5 BW, a timer would be started to record a temp sitting time. If the temp sitting time is longer than a time threshold (e.g., 2 s), sitting activity is recognized from the beginning of this time period. Similarly, when the measured total pressure is increased to a value larger than 0.5 BW, a timer would be started to record a temp standing time. If the temp standing time is longer than a time threshold (e.g., 2 s), standing activity is recognized from the beginning of this time period. In this article, an empirical threshold of 2 s was used for recognizing “sitting” and “standing.”

IV. EXPERIMENTS AND RESULTS

In this section, experiments were designed to evaluate the performance of gait parameters measurement and ADLs recognition. To evaluate the performance of “gait analysis in terms of ADLs,” an experiment with a sequence of ADLs was designed to simulate the scenarios in everyday life.

A. Accuracy of the Measured Gait Parameters

To evaluate the accuracy of the measured gait parameters, three experiments were designed to evaluate the measured temporal gait parameters, GRF, and turning related gait parameters, respectively.

1) *Accuracy of Temporal Gait Parameters:* From the description of the temporal gait parameters in Table I, it is obvious that the accuracy of all the temporal gait parameters, including “gait cycle time,” “step time,” “swing time,”

“stance time,” “single support time,” “double support time,” and “cadence” relies on the accuracy of the detected initial contact event and the last contact event. Since the initial contact event is the first sample of the stance phase and the last contact event is the last sample of the stance phase, both events were detected with the stance phase detection algorithm. In the experiment of evaluating the accuracy of the detected initial contact and last contact events, a subject wearing a pair of Smart Insole walked in his comfort speed for 20 steps. During the experiment, all the data from Smart Insoles was recorded with a smartphone. At the same time, feet activities of the subject were recorded with a video camera as ground truth for evaluating the accuracy of the detected initial contact and last contact events. Through comparing with the ground truth, the error of the detected initial contact and last contact events were 0.0 ± 14.1 ms and 5.2 ± 15.5 ms in terms of mean \pm standard deviation (std), respectively. Since the sample interval of the pressure sensor array was 33.3 ms, most of the initial contact and last contact events were detected with their nearest samples. In other words, initial contact and last contact events could be detected with the stance phase detection algorithm with a high accuracy. This could ensure the accuracy of the measured temporal gait parameters. For example, the error of gait cycle time, stance time, and swing time were 1.2 ± 14.9 ms, -3.5 ± 15.6 ms, and 5.2 ± 8.0 ms, respectively. For applications require a lower standard deviation, the sample rate could be increased to meet the requirement.

2) *Accuracy of Force Related Gait Parameters:* Accuracy of force related gait parameters are determined by the measured GRF. In this experiment, an AMTI OR6 series force plate was used as ground truth to evaluate the GRF measured by Smart Insole. Two different activities—“walking” and “running” were used to evaluate the reliability of GRF measurement across activities. At the first stage of the experiment, a subject wearing a pair of Smart Insole walked on the force plate in his comfort speed for 20 steps. Then the subject repeated the same process with the “running” activity. To align the data from Smart Insole and force plate, the subject started the experiment by kicking the force plate with his left heel to create a special signal that could mark the experiment start in the data from both devices.

To compare the GRF measured by force plate and Smart Insole, GRF of each step was normalized to [0 1]. Since the sample rate of force plate is 1000 Hz which is much higher than the 30 Hz sample rate of Smart Insole, GRF from the force plate was down-sampled to 30 Hz to avoid the differences caused by the sample rate. Fig. 9(a) and (b) shows the GRF from both force plate and Smart Insole during the stance phase of “walking” and “running,” respectively. It is obvious that patterns of the GRF measured with force plate and Smart Insole are similar for both “walking” and “running.” Correlation of the GRF from the force plate and Smart Insole was calculated with all the 20 steps for each activity, and the mean values were 0.989 for both activities. The results indicate that: 1) the patterns of GRF from Smart Insole and force plate are similar and 2) Smart Insole has a stable performance on GRF measurement across activities. In addition, from Fig. 9(a) and (b), it is obvious that there are some differences in the

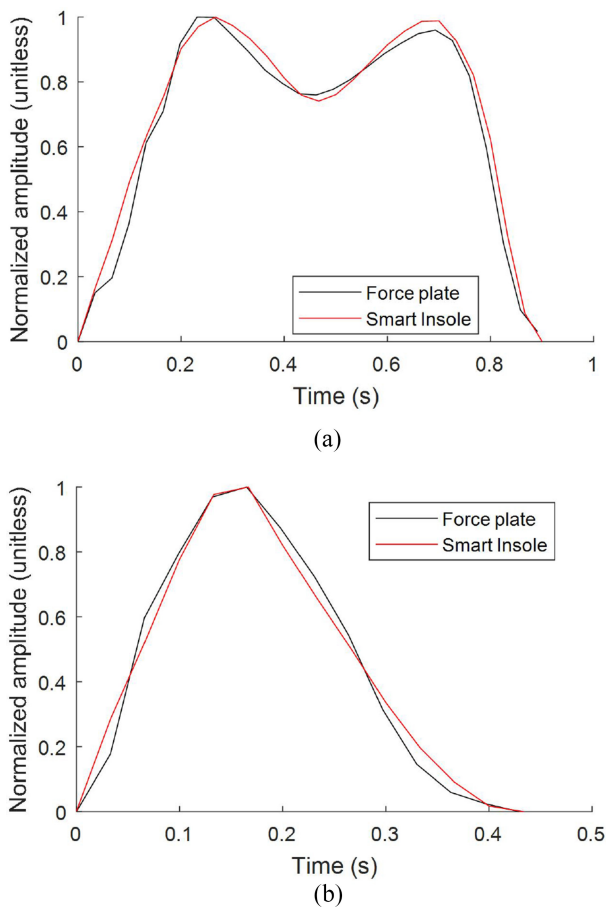


Fig. 9. Comparison of the GRF from Smart Insole and the force plate. (a) and (b) GRF during the stance phase of walking and running, respectively.

GRF measured by Smart Insole and force plate. One of the causes for the differences could be the fact that sensitivity of the piezo-resistive material is not perfectly uniform.

3) *Accuracy of Turning Related Gait Parameters*: Accuracy of the turning related gait parameters depends on two aspects: 1) the performance of the turning detection algorithm and 2) the accuracy of the measured turning angles. Therefore, the focus of this experiment is to evaluate these two aspects. The experiment setup is shown in Fig. 10(a). Two chairs were placed in the middle of a hallway, and the distance between these two chairs was about 5 m. Solid black lines indicate the straight walking path, and dashed lines indicate the turning path. Two arrows on the dashed lines indicate the walking direction. During the experiment, a subject walked around these two chairs in his comfort walking speed for 20 circles. Turning around one chair for one time, the subject would make a turn of 180° . Therefore, the subject made 40 times of 180° turning during the experiment.

Fig. 10(b) shows the turning angle of each step during ten continuous 180° turnings. Red points indicate the turning angle of each step. Green and blue triangles indicate the detected start and end of a turning event. The dashed line was the threshold for detecting a turning event. The experimental results showed that all the 40 turning events could be correctly detected. To evaluate the accuracy of the measured turning

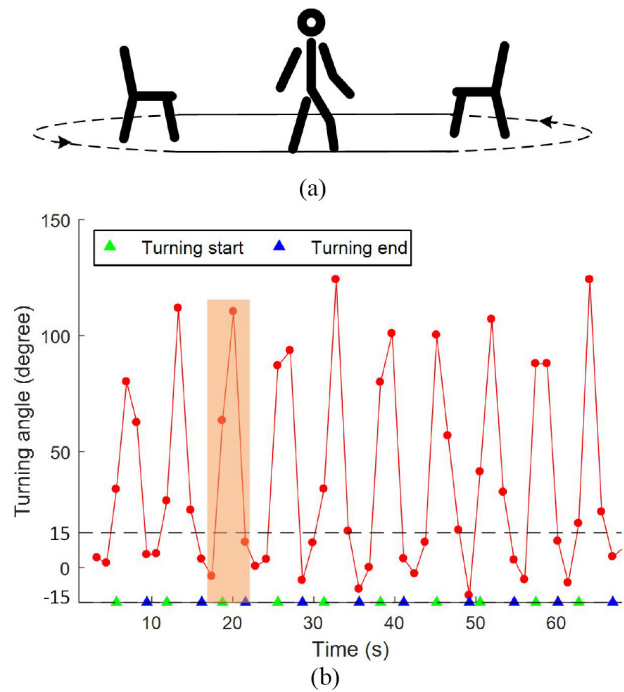


Fig. 10. Setup and results of the experiment for evaluating the turning related parameters. (a) Experiment setup. (b) Turning angle of each step during ten continuous 180° turnings. Red points indicate the turning angle of each step. Green and blue triangles indicate the detected start and end of a turning event. The dashed line indicates the threshold for detecting a turning event. Those four steps in the orange background were used to show an example of the steps between the end of two continuous turning events.

angles, the turning angle of all the steps between the end of two continuous turning events were added up and compared with the ground truth value which was 180° . Those four steps in the orange background shown in Fig. 10(b) is an example of the steps between the end of two continuous turning events. Finally, the total turning angle between the end of two continuous turnings was $178.07 \pm 9.46^\circ$ in terms of mean \pm std. The error of the mean value is 1.93° for a 180° turning, which is acceptable for most applications.

B. Accuracy of ADLs Recognition

Since different methods were proposed to recognize dynamic and quasi-static activities in Section III-C, two different experiments were designed accordingly to evaluate the performance of activity recognition methods.

To recognize dynamic activities, three features were extracted to train a linear SVM classification model. To avoid overfitting of the model over one subject, ten subjects were involved in this experiment. During the experiment, each subject wore a pair of Smart Insole and did each activity according to instructions. For “walking” and “running,” each subject did each activity along a straight hallway of about 30 m for three times. For “descend stairs” and “ascend stairs,” each subject did each activity along a stair of nine steps for 10 times. During the experiment, all the subjects used their comfort gait to perform different activities. To reduce potential disturbances introduced into the data set for model training and testing, only the strides in the middle of each experiment were

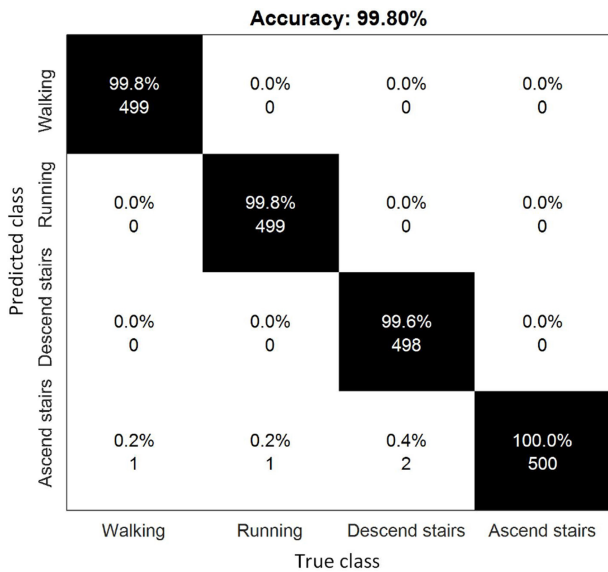


Fig. 11. Confusion matrix of the linear SVM model for dynamic activities recognition.

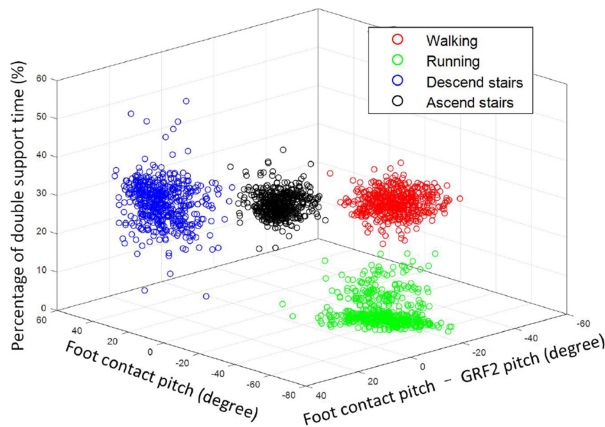


Fig. 12. Distribution of the dynamic activity in the space defined by “foot contact pitch,” “foot contact pitch—GRF2 pitch,” and “percentage of double support time.”

used for feature extraction. To keep the balance of the data set, 50 strides were used for feature extraction for each activity of each subject. Finally, there were 500 samples in the data set for each activity. The performance of the linear SVM classification model was evaluated with fivefold cross-validation.

The testing result was shown with a confusion matrix in Fig. 11. The accuracy of “walking,” “running,” “descend stairs,” and “ascend stairs” was 99.8%, 99.8%, 99.6%, and 100.0%, respectively. The overall accuracy is 99.8%. The high recognition accuracy across different activities indicates that the linear SVM model trained with these three features (i.e., “foot contact pitch,” “foot contact pitch—GRF2 pitch,” and “percentage of double support time”) could meet the requirement of recognizing dynamic activities. Fig. 12 provides an intuitive view of the distribution of “walking,” “running,” “descend stairs,” and “ascend stairs” in the space defined by all the three features. It is obvious that these four dynamic activities could be well separated by these three features.

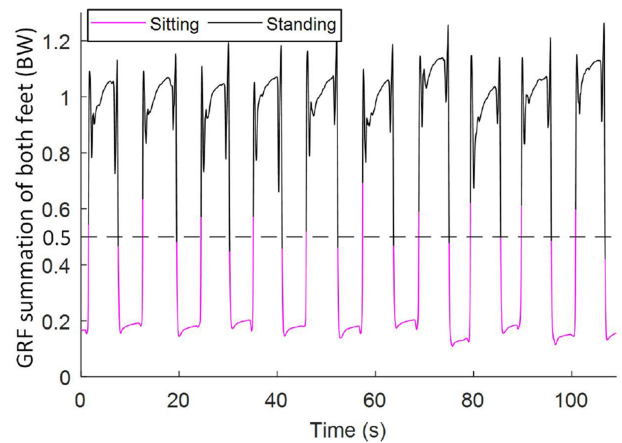


Fig. 13. GRF summation of both feet during “sitting” and “standing” activities. The dashed line indicates the threshold (0.5 BW) for recognizing “sitting” and “standing.” Magenta and black lines indicate the data corresponding to the recognized “sitting” and “standing” activities, respectively.

TABLE II
GENERALIZATION PERFORMANCE ACROSS PEOPLE

	Test1	Test2	Test3	Test4	Test5	Mean
Accuracy (%)	100.00	99.75	99.50	100.00	98.50	99.55

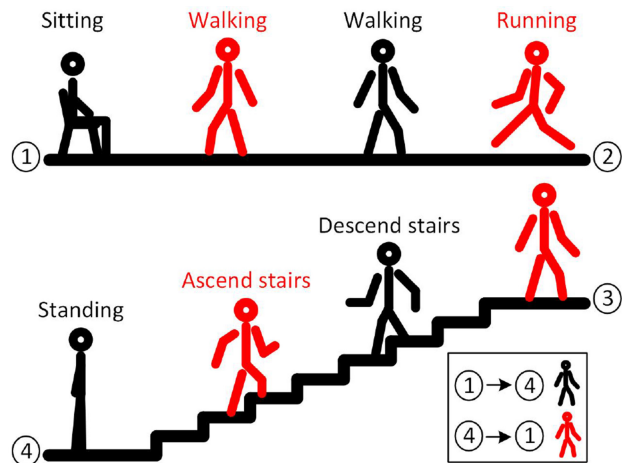


Fig. 14. Experiment for performance evaluation in practice. Circle one to circle four indicates four locations on the experiment path. Circle one and four indicate the start and end of the experiment path. Circle two and three indicate the end of the straight path and the start of stairs. From circle two to circle three, the subject should make one 90° turning and walk several steps. Black icon persons indicate the activities used to move from circle one location to circle four, and red icon persons indicate the activities used to move from circle four to circle one.

To evaluate the generalization performance of the method across people, fivefold cross-validation was done in terms of different subjects. Ten subjects were shuffled randomly, and split into five groups. For each test, the data of four groups of subjects were used for model training and the data of the remaining two groups of subjects was used for testing. As shown in Table II, accuracy of the tests from test 1 to test 5 was 100.00%, 99.75%, 99.50%, 100.00%, and 98.50%, respectively. The high accuracy across all these five tests indicates that the linear SVM model trained with these three features has a good generalization performance.

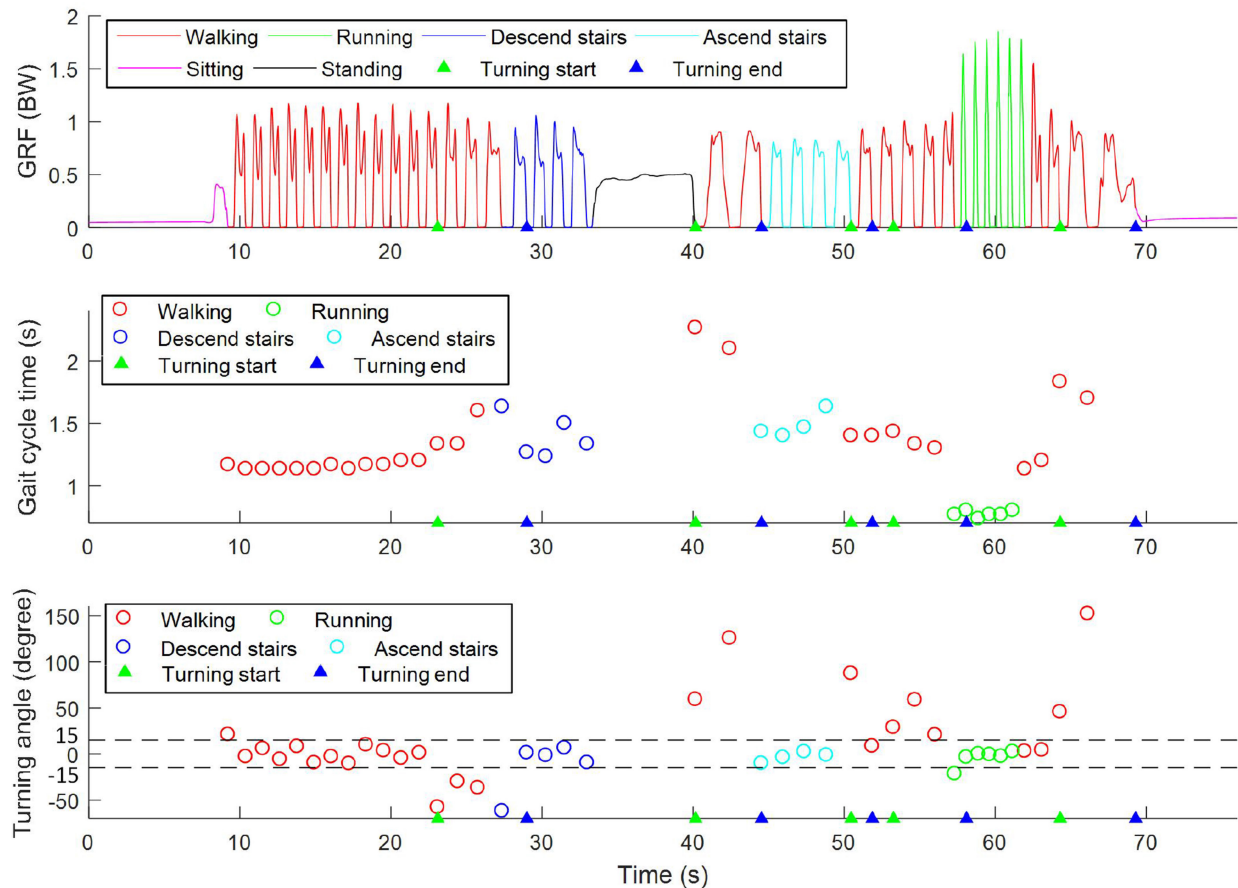


Fig. 15. Effect of “gait analysis in terms of ADLs” shown with “GRF,” “gait cycle time,” and “turning angle” measured during different ADLs. Different colors indicate the parameters measured during different activities.

In the experiment of evaluating the method for recognizing quasi-static activities (i.e., “sitting” and “standing”), a subject wore a pair of Smart Insole and performed both activities according to instructions. The experiment was started with a 5 s of sitting, subsequently, the subject stood up and kept standing for another 5 s, then he sat down and repeated the whole sitting-standing process for 20 times. At the same time, activities of the subject were recorded with a video camera as a ground truth. The experimental results showed that all the “sitting” and “standing” activities could be recognized correctly. Fig. 13 shows the GRF summation of both feet during ten continuous “sitting” and “standing” activities. The dashed line indicates the threshold (0.5 BW) for recognizing “sitting” and “standing.” The lines with magenta and black colors indicate the data corresponding to the recognized “sitting” and “standing,” respectively. It is obvious that “sitting” and “standing” activities have a significant difference on the GRF summation of both feet, and 0.5 BW is a suitable threshold to recognize these two activities.

C. Gait Analysis in Terms of ADLs—Performance Evaluation in Practice

To evaluate the performance of the “gait analysis in terms of ADLs” in practice, a subject wearing a pair of Smart Insoles performed a sequence of ADLs according to instructions. Fig. 14 shows the type of paths and activities involved in

the experiment. The path connecting circle one and circle two is a straight hallway, then a 90° turning on the path leads it to location circle three which is the start of stairs, and another 90° turning on circle three leads it to location circle four which is at the end of the stairs. Black icon persons indicate the activities used to move from circle one to circle four, and red icon persons indicate the activities moving in the reverse direction. The experiment sequence was as follows: 1) At the beginning of the experiment, the subject sat in the chair at location circle one for a while (about 8 s); 2) stood up and walked to location circle two, then made one 90° turning to turn the body face circle three; 3) walked to circle three, then made one 90° turning to turn the body face circle four; 4) walked downstairs and stood still for about 5 s; 5) turned around and walked upstairs to circle three, then made one 90° turning to turn the body face circle two; 6) walked to circle two, then made one 90° turning to turn the body face circle one; 7) run several steps, then changed to “walking” when near circle one; and 8) turned around in front of the chair and sat in the chair. During the experiment, activities of the subject were recorded with a video camera as a ground truth for performance analysis.

“Gait analysis in terms of ADLs” enables an intuitive method to present the comprehensive gait analysis results. As shown in Fig. 15, different colors were used to highlight the gait parameters acquired during different activities. For example, red and green colors indicate the gait parameters

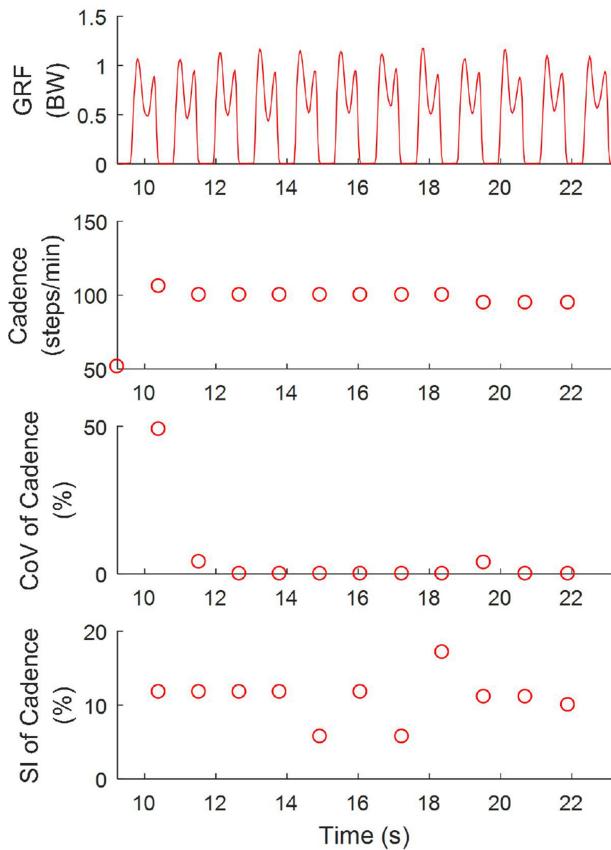


Fig. 16. Gait analysis in terms of straight walking. “GRF,” “Cadence,” “CoV of cadence,” and “SI of cadence” measured during straight walking were extracted to show the effect of gait analysis in term of one specific activity.

acquired during the recognized “walking” and “running” activities, respectively. In addition, green and blue triangles indicate the start and end of a turning event, respectively. “GRF,” “gait cycle time,” and “turning angle” of the left foot were taken as examples to show the effect of the “gait analysis in terms of ADLs.”

As discussed in Section III-B3, the variance of gait parameters is associated with falling, frailty, and neuro-degenerative diseases. However, except for diseases, other factors, such as the changes of activities, turning events, etc. could increase gait variance. As shown in Fig. 15, it is obvious that when the activity was changing from “walking” to “descend stairs,” the gait cycle time was different from normal walking or “descend stairs.” In addition, during the first turning event, the gait cycle time was significantly increased. With the help of “gait analysis in terms of ADLs,” it is easy for clinical professionals to see whether the changes of gait parameters were caused by activities or diseases.

Comprehensive results shown in Fig. 15 supply an intuitive view of the gait parameters measured during different activities. In addition to the comprehensive results, “gait analysis in terms of ADLs” makes it possible for clinical professionals to extract the gait parameters corresponding to any specific activity. As shown in Fig. 16, gait parameters corresponding to straight walking were extracted for analysis individually. “GRF,” “Cadence,” “CoV of cadence,” and “SI of cadence”

were taken as examples to show the gait parameters in the straight walking activity. Compared with the comprehensive view, gait analysis in terms of a specific activity could make it easy to get focus on the gait performance during one specific activity, and avoid the disturbance of other activities.

V. DISCUSSION

The experimental results showed the accuracy and reliability of the algorithms for gait parameters calculation and ADLs recognition. The experiment with a sequence of ADLs showed the ability of “gait analysis in terms of ADLs” to realize gait analysis in everyday life.

One advantage of “gait analysis in terms of ADLs” is to contribute to the disease diagnosis in early stages. Taking PD for example, for the early stages of PD, the symptoms of the disease are mild, and the locomotor and balance problems are negligible or absent [51]. However, PD patients demonstrated significant slower step and greater number of steps to finish a turn. In addition, for the early stages of PD, the amplitude of both GRF peaks is reduced. Through wearing Smart Insole in everyday life, the gait performance during different ADLs of a subject could be recorded and analyzed separately. For PD diagnosis, it is convenient to extract all the gait parameters measured during “turning” and analyze the turning performance with gait parameters, such as “turning steps,” “turning time,” “turning angle,” etc. Besides, to check the amplitude of both GRF peaks, “weight-acceptance force” and “push-off force” during the “walking” activity could be extracted for analysis individually.

In addition to gait parameters, “gait analysis in terms of ADLs” could also supply information about mobility which is important for clinical applications. Through monitoring ADLs continuously, changes of the mobility across the day and week, the response of the mobility to interventions, and the influence of environments on mobility could be measured [57]. Researches showed that mobility assessment in everyday life provides information about disease progression and the effectiveness of rehabilitation [58]. Moreover, the sequence of different ADLs in time could also reveal potential health problems. For example, “standing” or “sitting” in the middle of “ascend stairs” or “descend stairs” may indicate frail.

In this article, to show the ability of the Smart Insole to do researches about plantar pressure on the foot subareas, the pressure sensor array was segmented with the most popular used method into three areas: 1) forefoot; 2) midfoot; and 3) hindfoot according to the foot anatomy. Since there are 96 pressure sensors uniformly distributed on the sensor array, which ensures a high spatial resolution, the pressure sensor array could support different segmentation methods according to different research needs.

With the development of the Internet of Things (IoT) in the healthcare field, wearable technologies have shown the potential to monitor many other health related vital signals, such as electromyogram (EMG) [59] and ECG [60] in a free-living environment. However, similar to gait analysis, most of the published researches only focused on demonstrating the ability to measure signals in a free-living environment, but ignored an

important fact that the measured signals would be influenced by both diseases and ADLs. Without knowing the corresponding activities, the measured signals cannot be used for clinical applications. To address this problem, the method—“gait analysis in terms of ADLs” could be applied to these health related signals and realized physiological parameters monitoring in terms of ADLs.

VI. CONCLUSION

In this article, a novel gait analysis method—“gait analysis in terms of ADLs”—was proposed to realize gait analysis in everyday life. Twenty six gait parameters were extracted to show the ability of Smart Insole to realize a comprehensive gait analysis. A novel activity recognition algorithm was proposed based on characteristics of human gait, which realized a high recognizing accuracy with low computation load. Compared with the traditional wearable gait analysis methods, “gait analysis in terms of ADLs” could not only measure gait parameters during ADLs, but also indicate the activities of the measured parameters, which makes the measure gait parameters understandable for clinical professionals.

REFERENCES

- [1] M. W. Whittle, *Gait Analysis: An Introduction*. Oxford, U.K.: Butterworth-Heinemann, 2014.
- [2] J. M. Hausdorff, M. E. Cudkovicz, R. Firtion, J. Y. Wei, and A. L. Goldberger, “Gait variability and basal ganglia disorders: Stride-to-stride variations of gait cycle timing in Parkinson’s disease and Huntington’s disease,” *Movement Disord.*, vol. 13, no. 3, pp. 428–437, 1998.
- [3] D. Podsiadlo and S. Richardson, “The timed ‘Up & Go’: A test of basic functional mobility for frail elderly persons,” *J. Amer. Geriatr. Soc.*, vol. 39, no. 2, pp. 142–148, 1991.
- [4] F. Malouin, “Observational gait analysis: Normal and pathological function,” in *Gait Analysis, Theory and Application*, R. L. Craik and C. A. Oatis, Eds. St. Louis, MO, USA: Mosby, 1995, pp. 112–124.
- [5] J. J. Brunnekreef, C. J. Van Uden, S. Van Moorsel, and J. G. Kooloos, “Reliability of videotaped observational gait analysis in patients with orthopedic impairments,” *BMC Musculoskeletal Disord.*, vol. 6, no. 1, p. 17, 2005.
- [6] M. E. Eastlack, J. Arvidson, L. Snyder-Mackler, J. V. Danoff, and C. L. McGarvey, “Interrater reliability of videotaped observational gait-analysis assessments,” *Phys. Therapy*, vol. 71, no. 6, pp. 465–472, 1991.
- [7] R. W. Kressig, O. Beauchet, “Guidelines for clinical applications of spatio-temporal gait analysis in older adults,” *Aging Clin. Exp. Res.*, vol. 18, no. 2, pp. 174–176, 2006.
- [8] C. Zampieri, A. Salarian, P. Carlson-Kuhta, J. G. Nutt, and F. B. Horak, “Assessing mobility at home in people with early Parkinson’s disease using an instrumented timed up and go test,” *Parkinsonism Related Disord.*, vol. 17, no. 4, pp. 277–280, 2011.
- [9] A. Galan-Mercant and A. Cuesta-Vargas, “Clinical frailty syndrome assessment using inertial sensors embedded in smartphones,” *Physiol. Meas.*, vol. 36, no. 9, pp. 1929–1942, 2015.
- [10] O. Beauchet, G. Allali, M. Montero-Odasso, E. Sejdic, B. Fantino, and C. Annweiler, “Motor phenotype of decline in cognitive performance among community-dwellers without dementia: Population-based study and meta-analysis,” *PLOS ONE*, vol. 9, no. 6, 2014, Art. no. e99318.
- [11] A. Muro-De-La-Herran, B. Garcia-Zapirain, and A. Mendez-Zorrilla, “Gait analysis methods: An overview of wearable and non-wearable systems, highlighting clinical applications,” *Sensors*, vol. 14, no. 2, pp. 3362–3394, 2014.
- [12] C. Prakash, K. Gupta, A. Mittal, R. Kumar, and V. Laxmi, “Passive marker based optical system for gait kinematics for lower extremity,” *Procedia Comput. Sci.*, vol. 45, pp. 176–185, Mar. 2015.
- [13] Y. Wang, J. Sun, J. Li, and D. Zhao, “Gait recognition based on 3D skeleton joints captured by Kinect,” in *Proc. IEEE Int. Conf. Image Process. (ICIP)*, 2016, pp. 3151–3155.
- [14] T. Dutta, “Evaluation of the Kinect™ sensor for 3-D kinematic measurement in the workplace,” *Appl. Ergonom.*, vol. 43, no. 4, pp. 645–649, 2012.
- [15] H. Jagos *et al.*, “Mobile gait analysis via eSHOEs instrumented shoe insoles: A pilot study for validation against the gold standard GAITrite®,” *J. Med. Eng. Technol.*, vol. 41, no. 5, pp. 375–386, 2017.
- [16] H. Lau and K. Tong, “The reliability of using accelerometer and gyroscope for gait event identification on persons with dropped foot,” *Gait Posture*, vol. 27, no. 2, pp. 248–257, 2008.
- [17] X. Meng, H. Yu, and M. P. Tham, “Gait phase detection in able-bodied subjects and dementia patients,” in *Proc. 35th Annu. Int. Conf. IEEE Eng. Med. Biol. Soc. (EMBC)*, 2013, pp. 4907–4910.
- [18] Tekscan. *F-Scan System*. Accessed: Oct. 16, 2019. [Online]. Available: <https://www.tekscan.com/products-solutions/systems/f-scan-system>
- [19] R. Steele, A. Lo, C. Secombe, and Y. K. Wong, “Elderly persons’ perception and acceptance of using wireless sensor networks to assist healthcare,” *Int. J. Med. Informat.*, vol. 78, no. 12, pp. 788–801, 2009.
- [20] M. Saito *et al.*, “An in-shoe device to measure plantar pressure during daily human activity,” *Med. Eng. Phys.*, vol. 33, no. 5, pp. 638–645, 2011.
- [21] B. Wang, K. S. Rajput, W.-K. Tam, A. K. Tung, and Z. Yang, “FreeWalker: A smart insole for longitudinal gait analysis,” in *Proc. 37th Annu. Int. Conf. IEEE Eng. Med. Biol. Soc. (EMBC)*, 2015, pp. 3723–3726.
- [22] Arion. *Arion Smart Insoles 2.0*. Accessed: Oct. 16, 2019. [Online]. Available: <https://www.arion.run/product/arion-smart-insoles-2-0/>
- [23] ReTiSense. *Stridalyzer Prism Sensor Insoles*. Accessed: Oct. 16, 2019. [Online]. Available: <http://retisense.com/product/stridalyzer-prism-sensor-insoles/>
- [24] EeonTex. *Eeontex Nonwoven Pressure Sensing Fabric*. Accessed: Oct. 15, 2019. [Online]. Available: <https://cdn.sparkfun.com/datasheets/E-Textiles/Materials/NW170-SLPA-2k>
- [25] D. Chen, Y. Cai, and M.-C. Huang, “Customizable pressure sensor array: Design and evaluation,” *IEEE Sensors J.*, vol. 18, no. 15, pp. 6337–6344, Aug. 2018.
- [26] D. Chen *et al.*, “Smart insole-based indoor localization system for Internet of Things applications,” *IEEE Internet Things J.*, vol. 6, no. 4, pp. 7253–7265, Aug. 2019.
- [27] S. Crea, M. Donati, S. De Rossi, C. Oddo, and N. Vitiello, “A wireless flexible sensorized insole for gait analysis,” *Sensors*, vol. 14, no. 1, pp. 1073–1093, 2014.
- [28] J. Perry and J. R. Davids, “Gait analysis: Normal and pathological function,” *J. Pediatric Orthopaedics*, vol. 12, no. 6, p. 815, 1992.
- [29] D. A. Winter, *Biomechanics and Motor Control of Human Gait: Normal, Elderly and Pathological*. Waterloo, ON, Canada: Waterloo Biomech., 1991.
- [30] S. H. Koozekanani, M. T. Balmaseda, Jr., M. T. Fatehi, and E. D. Lowney, “Ground reaction forces during ambulation in Parkinsonism: Pilot study,” *Archives Phys. Med. Rehabil.*, vol. 68, no. 1, pp. 28–30, 1987.
- [31] E. Ueno, N. Yanagisawa, and M. Takami, “Gait disorders in Parkinsonism. A study with floor reaction forces and EMG,” *Adv. Neurol.*, vol. 60, pp. 414–418, Dec. 1992.
- [32] A. Caselli, H. Pham, J. M. Giurini, D. G. Armstrong, and A. Veves, “The forefoot-to-rearfoot plantar pressure ratio is increased in severe diabetic neuropathy and can predict foot ulceration,” *Diabetes Care*, vol. 25, no. 6, pp. 1066–1071, 2002.
- [33] A. Ruhe, R. Fejer, and B. Walker, “Center of pressure excursion as a measure of balance performance in patients with non-specific low back pain compared to healthy controls: A systematic review of the literature,” *Eur. Spine J.*, vol. 20, no. 3, pp. 358–368, 2011.
- [34] K. J. Chesnin, L. Selby-Silverstein, and M. P. Besser, “Comparison of an in-shoe pressure measurement device to a force plate: Concurrent validity of center of pressure measurements,” *Gait Posture*, vol. 12, no. 2, pp. 128–133, 2000.
- [35] M. Q. Liu, F. C. Anderson, M. G. Pandey, and S. L. Delp, “Muscles that support the body also modulate forward progression during walking,” *J. Biomech.*, vol. 39, no. 14, pp. 2623–2630, 2006.
- [36] K. E. Zelik and A. D. Kuo, “Human walking isn’t all hard work: Evidence of soft tissue contributions to energy dissipation and return,” *J. Exp. Biol.*, vol. 213, no. 24, pp. 4257–4264, 2010.
- [37] A. De Cock, D. De Clercq, T. Willems, and E. Witvrouw, “Temporal characteristics of foot roll-over during barefoot jogging: Reference data for young adults,” *Gait Posture*, vol. 21, no. 4, pp. 432–439, 2005.
- [38] C. W. Chan and A. Rudins, “Foot biomechanics during walking and running,” in *Proc. Mayo Clinic*, vol. 69, 1994, pp. 448–461.

- [39] H. Yu, J. Riskowski, R. Brower, and T. Sarkodie-Gyan, "Gait variability while walking with three different speeds," in *Proc. IEEE Int. Conf. Rehabil. Robot.*, 2009, pp. 823–827.
- [40] F. Ayoubi, C. P. Launay, C. Annweiler, and O. Beauchet, "Fear of falling and gait variability in older adults: A systematic review and meta-analysis," *J. Amer. Med. Directors Assoc.*, vol. 16, no. 1, pp. 14–19, 2015.
- [41] J. M. Hausdorff, D. A. Rios, and H. K. Edelberg, "Gait variability and fall risk in community-living older adults: A 1-year prospective study," *Archives Phys. Med. Rehabil.*, vol. 82, no. 8, pp. 1050–1056, 2001.
- [42] B. E. Maki, "Gait changes in older adults: Predictors of falls or indicators of fear," *J. Amer. Geriatr. Soc.*, vol. 45, no. 3, pp. 313–320, 1997.
- [43] J. M. Hausdorff, "Gait variability: Methods, modeling and meaning," *J. Neuroeng. Rehabil.*, vol. 2, no. 1, p. 19, 2005.
- [44] N. Herssens, E. Verbecque, A. Hallemans, L. Vereeck, V. Van Rompaey, and W. Saeys, "Do spatiotemporal parameters and gait variability differ across the lifespan of healthy adults? A systematic review," *Gait Posture*, vol. 64, pp. 181–190, Jul. 2018.
- [45] K. K. Patterson *et al.*, "Gait asymmetry in community-ambulating stroke survivors," *Archives Phys. Med. Rehabil.*, vol. 89, no. 2, pp. 304–310, 2008.
- [46] R. Baltadjieva, N. Giladi, L. Gruendlinger, C. Peretz, and J. M. Hausdorff, "Marked alterations in the gait timing and rhythmicity of patients with de novo Parkinson's disease," *Eur. J. Neurosci.*, vol. 24, no. 6, pp. 1815–1820, 2006.
- [47] K. K. Patterson, W. H. Gage, D. Brooks, S. E. Black, and W. E. McIlroy, "Evaluation of gait symmetry after stroke: A comparison of current methods and recommendations for standardization," *Gait Posture*, vol. 31, no. 2, pp. 241–246, 2010.
- [48] B. Burkett, J. Smeathers, and T. Barker, "Walking and running inter-limb asymmetry for Paralympic trans-femoral amputees, a biomechanical analysis," *Prosthetics Orthotics Int.*, vol. 27, no. 1, pp. 36–47, 2003.
- [49] C. L. Christiansen and J. E. Stevens-Lapsley, "Weight-bearing asymmetry in relation to measures of impairment and functional mobility for people with knee osteoarthritis," *Archives Phys. Med. Rehabil.*, vol. 91, no. 10, pp. 1524–1528, 2010.
- [50] L. Jørgensen, N. J. Crabtree, J. Reeve, and B. K. Jacobsen, "Ambulatory level and asymmetrical weight bearing after stroke affects bone loss in the upper and lower part of the femoral neck differently: Bone adaptation after decreased mechanical loading," *Bone*, vol. 27, no. 5, pp. 701–707, 2000.
- [51] P. Creenna, "The association between impaired turning and normal straight walking in Parkinson's disease," *Gait Posture*, vol. 26, no. 2, pp. 172–178, 2007.
- [52] N. Hegde, M. Bries, T. Swibas, E. Melanson, and E. Sazonov, "Automatic recognition of activities of daily living utilizing insole-based and wrist-worn wearable sensors," *IEEE J. Biomed. Health Inform.*, vol. 22, no. 4, pp. 979–988, Jul. 2017.
- [53] E. S. Sazonov, G. Fulk, J. Hill, Y. Schutz, and R. Browning, "Monitoring of posture allocations and activities by a shoe-based wearable sensor," *IEEE Trans. Biomed. Eng.*, vol. 58, no. 4, pp. 983–990, Apr. 2011.
- [54] S. Pirttikangas, K. Fujinami, and T. Nakajima, "Feature selection and activity recognition from wearable sensors," in *Proc. Int. Symp. Ubiquitous Comput. Syst.*, 2006, pp. 516–527.
- [55] R. Riener, M. Rabuffetti, and C. Frigo, "Stair ascent and descent at different inclinations," *Gait Posture*, vol. 15, no. 1, pp. 32–44, 2002.
- [56] T. F. Novacheck, "The biomechanics of running," *Gait Posture*, vol. 7, no. 1, pp. 77–95, 1998.
- [57] F. Horak, L. King, and M. Mancini, "Role of body-worn movement monitor technology for balance and gait rehabilitation," *Phys. Therapy*, vol. 95, no. 3, pp. 461–470, 2015.
- [58] M. Mancini *et al.*, "Continuous monitoring of turning in Parkinson's disease: Rehabilitation potential," *NeuroRehabilitation*, vol. 37, no. 1, pp. 3–10, 2015.
- [59] A. S. Kundu, O. Mazumder, and S. Bhaumik, "Design of wearable, low power, single supply surface EMG extractor unit for wireless monitoring," in *Proc. 2nd Int. Conf. Nanotechnol. Biosensors*, 2011, pp. 69–74.
- [60] E. Nemati, M. J. Deen, and T. Mondal, "A wireless wearable ECG sensor for long-term applications," *IEEE Commun. Mag.*, vol. 50, no. 1, pp. 36–43, Jan. 2012.